AGU PUBLICATIONS

JGR

Journal of Geophysical Research: Earth Surface

RESEARCH ARTICLE

10.1002/2014JF003308

Key Points:

- Bed load transport flux shows timescale-dependent fluctuations with scale breaks
- These breaks define three regimes: intermittent, invariant, and memoryless
- Theory explains regimes via particle discreteness and correlated particle motion

Correspondence to:
X. Fu,
xdfu@tsinghua.edu.cn

Citation:
Ma, H., J. Heyman, X. Fu, F. Mettra, C. Ancey, and G. Parker (2014), Bed load transport over a broad range of timescales: Determination of three regimes of fluctuations, *J. Geophys. Res. Earth Surf.*, *119*, 2653–2673, doi:10.1002/2014JF003308.

Received 11 AUG 2014
Accepted 3 NOV 2014
Accepted article online 5 NOV 2014
Published online 17 DEC 2014

Bed load transport over a broad range of timescales: Determination of three regimes of fluctuations

Hongbo Ma[1], Joris Heyman[2], Xudong Fu[1], Francois Mettra[2], Christophe Ancey[2], and Gary Parker[3]

[1]State Key Laboratory of Hydroscience and Engineering, Department of Hydraulic Engineering, Tsinghua University, Beijing, China, [2]School of Architecture, Civil and Environmental Engineering, École Polytechnique Fédérale de Lausanne, Lausanne, Switzerland, [3]Department of Civil and Environmental Engineering and Department of Geology, University of Illinois, Urbana, Illinois, USA

Abstract This paper describes the relationship between the statistics of bed load transport flux and the timescale over which it is sampled. A stochastic formulation is developed for the probability distribution function of bed load transport flux, based on the Ancey et al. (2008) theory. An analytical solution for the variance of bed load transport flux over differing sampling timescales is presented. The solution demonstrates that the timescale dependence of the variance of bed load transport flux reduces to a three-regime relation demarcated by an intermittency timescale (t_I) and a memory timescale (t_c). As the sampling timescale increases, this variance passes through an intermittent stage ($\ll t_I$), an invariant stage ($t_I < t < t_c$), and a memoryless stage ($\gg t_c$). We propose a dimensionless number (Ra) to represent the relative strength of fluctuation, which provides a common ground for comparison of fluctuation strength among different experiments, as well as different sampling timescales for each experiment. Our analysis indicates that correlated motion and the discrete nature of bed load particles are responsible for this three-regime behavior. We use the data from three experiments with high temporal resolution of bed load transport flux to validate the proposed three-regime behavior. The theoretical solution for the variance agrees well with all three sets of experimental data. Our findings contribute to the understanding of the observed fluctuations of bed load transport flux over monosize/multiple-size grain beds, to the characterization of an inherent connection between short-term measurements and long-term statistics, and to the design of appropriate sampling strategies for bed load transport flux.

1. Introduction

Bed load transport plays an important role in river morphology, desertification, and landscape evolution, and is also a contributor to the average long-term sediment budget. The prediction of bed load transport has been the topic of intensive research over the last century. However, state-of-the-art, macroscopically averaged formulas may still predict bed load transport rates that deviate by as much as 1 and 2 orders of magnitude from field data in mountain streams and aeolian systems [*Barchyn et al.*, 2014; *Barry*, 2004; *Gomez and Church*, 1989; *Martin*, 2003; *Sherman and Li*, 2012; *Wilcock*, 2001]. This renders the long-term prediction of river morphology and desert landscape very difficult. The specific evolution of a given area over a specified period may significantly differ from the mean trend, and this difference depends in part on the magnitude of fluctuations in bed load flux [e.g., *Phillips*, 2010, 2011].

The fluctuation of bed load transport flux has received increasing attention in terms of microscale (particle scale) mechanisms and statistical characterization [*Ancey and Heyman*, 2014; *Heyman et al.*, 2014; *Singh et al.*, 2009]. In this regard, these fluctuations show stochasticity [*Ancey et al.*, 2006; *Bohm et al.*, 2004; *Frey et al.*, 2003; *Furbish et al.*, 2012; *Heyman et al.*, 2013; *Turowski*, 2011], nonlocality [*Bradley et al.*, 2010; *Ganti et al.*, 2010; *Martin et al.*, 2012; *Nikora et al.*, 2002], and dependence on broad scales [*Bunte and Abt*, 2005; *Campagnol et al.*, 2012; *Ergenzinger et al.*, 1994; *Gomez et al.*, 1989; *Hoey*, 1992; *Martin et al.*, 2013; *Recking et al.*, 2012; *Singh et al.*, 2009]. Among the characteristics of bed load transport flux, scale dependence is of specific interest to geophysicists and engineers, since it is crucial for connecting results from short-term experiments and field surveys relevant to the prediction of the long-term evolution of river morphology and desert landscape [*Foufoula-Georgiou and Stark*, 2010].

The issue of scale-dependent statistics of bed load transport flux arises from the stochastic nature of bed load transport dynamics that purely deterministic models fail to capture. In general, if a power law relation exists between the variance of a fluctuating quantity and scale, it can be applied in a simple and elegant way so that measurements conducted at one scale can be easily extended to predict measurements at another scale. A power law characterizing the relationship between the variance of bed load transport flux and sampling timescale with scaling exponent -1 was proposed in the classical Einstein model, in which probabilistic concepts were first applied to the study of bed load transport [*Einstein*, 1937]. *Ancey et al*. [2006] recast Einstein's model into an equivalent Eulerian model that also results in a power law. Recent experiments have shown that a power law holds locally between the fluctuations of bed load transport flux and different time intervals [*Campagnol et al*., 2012; *Singh et al*., 2009]. However, the existence of a global power law relation between the statistics of bed load transport flux and sampling timescale has not been demonstrated with experimental data to date. (See *Stumpf and Porter* [2012] for a presentation of the mathematical criteria for the existence of such a relation.)

There is, on the other hand, experimental evidence suggesting a scale relation that is more complex than a power law. *Hamamori* [1962] and *Carey and Hubbell* [1986] attributed bed load transport fluctuation to bed form migration and obtained a timescale invariant formula for the probability distribution function of bed load transport flux. *Gomez et al*. [1989] compared bed load transport flux samples measured at different timescales and showed that the cumulative distribution function of the bed load transport flux has a dependency on the timescale. *Campagnol et al*. [2012] considered the process of bed load transport at fine scale and demonstrated the existence of a break in the power law relation at small sampling timescales.

The controversial question as to how the statistics of bed load transport vary over different sampling timescales motivates us to seek a comprehensive understanding of the dependence of bed load transport flux on scale. We first propose a theoretical formulation for the full-scale probability distribution function (PDF) of bed load transport flux, based on the theory of *Ancey et al*. [2008]. This theory can not only resolve the discreteness of bed load particles but can also characterize long-term autocorrelation associated with the number of moving particles. We show that the relation between the variance of fluctuations of bed load transport flux and sampling timescale can be analytically divided into three piecewise power law scaling relations. Three sets of experimental data available in the literature are used to test the theory, as well as to characterize the multiregime behavior associated with these scaling breaks.

The present study is organized as follows. Section 2 presents the theoretical formulation of the PDF of bed load transport flux and the resulting analytical solution for the variance of bed load transport flux over different sampling timescales. A dimensionless number is proposed to mathematically characterize this multiregime relation. Section 3 outlines the experimental evidence for this multiregime relation. This evidence is used to test the analytical formulation derived in section 2. Section 4 discusses the physical origin of the key parameters governing the multiregime relation and the implications of experimental results. In section 5 we summarize our findings and discuss the implications of the multiregime formulation, as well as its potential implication for future studies.

2. Development of Physics-Based Stochastic Theory of Bed Load Transport

We propose a physics-based formulation of the PDF of bed load transport flux over different sampling timescales and then derive an analytical expression of its variance so as to characterize its relation to sampling timescale. The formulation is based on the *Ancey et al*. [2008] stochastic theory, a schematic diagram of which is shown in Figure 1. *Ancey et al*. [2008] considered the number of moving particles $N(t) \in \{0, 1, 2, \cdots\}$ in a fixed observation window along the streamwise direction. In their study, $N(t)$ is the concerned random variable; it evolves in time according to a birth-death Markov process (Figure 1). The static bed reservoir of particles, which we here denote by the label B in Figure 1, is assumed to have an infinite capacity. Furthermore, S is the number of particles leaving the window. Let $P(n; t)$ denote the probability of $N(t) = n$. The probabilistic evolution of $N(t)$ results from the following transition events: (1) A moving particle enters the window from upstream at rate λ_0 [T^{-1}] in dt, i.e., $P(n \to n+1; \mathrm{d}t) = \lambda_0 \mathrm{d}t + o(\mathrm{d}t)$; (2) each moving particle leaves the window independently at emigration rate γ in dt such that the total emigration rate is γN [T^{-1}], i.e., $P(n \to n-1; \mathrm{d}t) = n\gamma \mathrm{d}t + o(\mathrm{d}t)$; (3) each moving particle settles independently onto the bed in the window at deposition rate σ in dt, such that the total deposition rate is σN [T^{-1}], i.e., $P(n \to n-1; \mathrm{d}t) = n\sigma \mathrm{d}t + o(\mathrm{d}t)$; (4) a resting particle can be dislodged from the bed by the fluid at a rate λ_1 [T^{-1}], i.e., $P(n \to n+1; \mathrm{d}t) = \lambda_1 \mathrm{d}t + o(\mathrm{d}t)$; and (5) each moving particle can destabilize a resting particle and set it moving at rate μ [T^{-1}], i.e., $P(n \to n+1; \mathrm{d}t) = n\mu \mathrm{d}t + o(\mathrm{d}t)$.

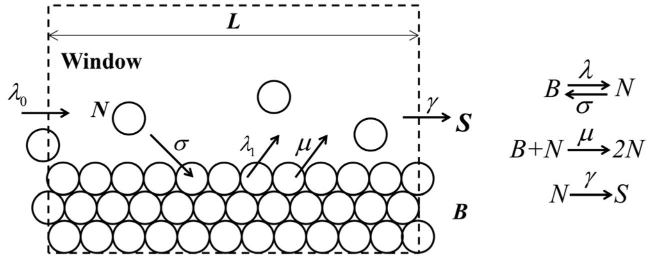

Figure 1. Sketch of definitions for the stochastic theory of bed load transport. *N* is the number of moving particles, and *B* is the number of particles in the granular bed. *S* represents the number of emigrating particles. Transition events can occur as follows: (1) a rest particle can be entrained individually by the water flow at rate λ_1; (2) a rest particle can be destabilized and moved by any moving particle at rate μ independently, i.e., total entrainment rate $f_1(N) = \lambda_1 + \mu N[\mathrm{T}^{-1}]$; (3) any moving particle can independently settle down to rest at rate σ, i.e., total deposition rate $f_2(N) = \sigma N[\mathrm{T}^{-1}]$; and (4) any moving particle can leave the window at rate γ independently, i.e., total emigration rate $f_3(N) = \gamma N[\mathrm{T}^{-1}]$; and (5) particles enter the window from upstream with a rate λ_0, which is merged with λ_1 into $\lambda = \lambda_0 + \lambda_1$ in the present study, as is $f_1(N) = \lambda + \mu N[\mathrm{T}^{-1}]$.

Ancey et al. [2006, 2008] experimentally demonstrated the fifth type of transition and described it as collective entrainment. A master equation governing the evolution of $P(n; t)$ was derived in *Ancey et al.* [2008],

$$\frac{\partial}{\partial t}P(n;t) = [\lambda + \mu(n-1)]P(n-1;t) + (\sigma+\gamma)(n+1)P(n+1;t) - [\lambda + (\mu+\sigma+\gamma)n]P(n;t) \tag{1a}$$

$$\frac{\partial}{\partial t}P(0;t) = (\sigma+\gamma)P(1;t) - \lambda P(0;t) \tag{1b}$$

where $\lambda = \lambda_0 + \lambda_1$. *Ancey et al*. [2008] showed that derived from equations (1a) and (1b), the PDF of number of the moving particle at steady state is a negative binomial distribution with mean value $\lambda/(\sigma+\gamma-\mu)$ and variance $\lambda(\sigma+\gamma)/(\sigma+\gamma-\mu)^2$, and that this solution accurately characterizes the fluctuation of number of moving particles in a given observational window.

It is worth noting that all four parameters λ, μ, σ, and γ have a physical meaning. Both σ and γ can be observed directly from imaging techniques. Let *L* and *W* denote the length of the observation window and the channel width, both with unit (L), and $\bar{u}_s$ be the average velocity of moving particles with unit (LT^{-1}). The parameter γ in the equilibrium state can be estimated as $\bar{u}_s/L$ [*Ancey*, 2010]. The individual entrainment rate λ_1 should be proportional to bed area, i.e., $\lambda_1 \sim O(LW)$, whereas μ and σ are independent of it. The parameters λ_1 and μ are, however, difficult to determine separately by image analysis and need to be calibrated using other statistical information. Thus, the mean number of moving particles, expressed as $\langle N \rangle = \lambda/(\sigma+\gamma-\mu) \sim O(LW)$ and the mean flux, expressed as $\langle \gamma N \rangle \sim O(W\bar{u}_s)$, are consistent with their corresponding physical definitions. Accordingly, the total entrainment rate is $f_1(N) = \lambda + \mu N \sim O(LW)$, the total deposition rate is $f_2(N) = \sigma N \sim O(LW)$, and the total emigration rate is $f_3(N) = \gamma N \sim O(\bar{u}_s W)$. Here $\bar{u}_s$ and *W* are constant in any particular case, while *L* can vary according to the size of the observation window from a small value up to the limiting streamwise geometry boundary (channel length).

In the *Ancey et al*. [2008] model, the collective entrainment rate μ is a crucial parameter for describing large fluctuations of *N*. If $\mu = 0$, $\mathrm{var}(N) = \mathrm{mean}(N) = \lambda/(\sigma+\gamma)$, and the statistics of *N* are described by a Poisson distribution, as is the increment number of emigrating particles *S* in a time period. However, as $\mu \to \sigma + \gamma$, var $(N) \gg \mathrm{mean}(N)$ and the fluctuation of *N* is large. A large value of μ allows a long-term autocorrelation of *N*, as presented below. It is worth noting that the original Einstein model [*Einstein*, 1937, 1950] can be interpreted as a special case of the *Ancey et al.* [2008] model with $\mu = 0$.

We are concerned here with the statistics of the bed load transport flux over a broad range of timescales. Recall that *Ancey et al*. [2008] focused on the statistics of the number of moving particles, while *Heyman et al*. [2013] were interested in the statistics of waiting time between particles leaving the window. No governing relation has been previously presented, however, for the evolution of particle flux in time. We derive such a relation below, in this section. More specifically, we derive the probability density function and variance of the bed load transport flux as a function of sampling time.

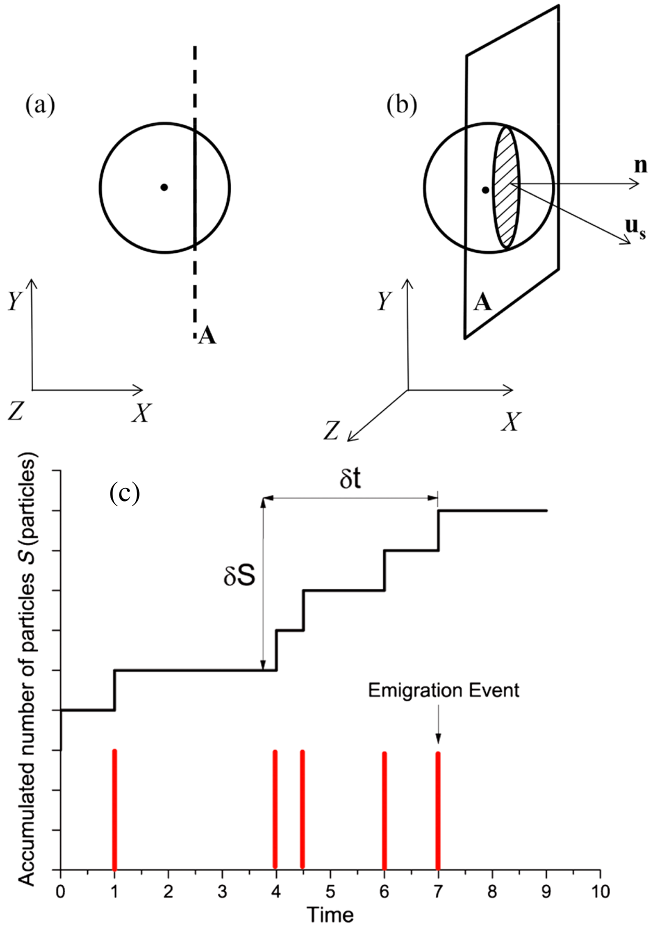

Figure 2. Schematic diagram of the definition of bed load transport flux. (a) Vertical plan. X is the streamwise direction, Y is the vertical direction, and Z is the spanwise direction. (b) Perspective view. The unit normal vector of the cross-section A is $\mathbf{n}$, and $\mathbf{u_s}$ is the velocity vector of the particle. (c) A sketch of the definition of bed load transport flux. Counts of accumulated particle numbers describe emigration events, which occur when particles pass through a cross section at specified time points. The bedload transport flux is defined as the increment of accumulated particle numbers between two times, i.e., δS divided by the temporal increment δt.

As shown in Figures 2a and 2b, the instantaneous volume flux of bed load transport can be defined as

$$Q_s(t) = \iint_A \mathbf{u_s} \cdot \mathbf{n} \mathrm{d}A \tag{2}$$

where $\mathbf{u_s}$ is the velocity vector and $\mathbf{n}$ is the unit normal vector of cross-section A. When conducting experiments and field survey, several factors in equation (2) are difficult to measure [*Ancey*, 2010; *Ballio et al.*, 2014]. Thus, the time-averaged flux of bed load transport is usually used instead of the instantaneous value [*Ancey*, 2010; *Ballio et al.*, 2014; *Campagnol et al.*, 2012; *Singh et al.*, 2009],

$$\begin{aligned} Q_s(t;\delta t) &= \frac{\int_t^{t+\delta t} Q_s(\tau)\mathrm{d}\tau}{\delta t} \\ &= \frac{\iint_A \int_t^{t+\delta t} \mathbf{u_s} \cdot \mathbf{n} \mathrm{d}\tau \mathrm{d}A}{\delta t} \\ &= \frac{\delta V_s}{\delta t} = v_s \frac{\delta S(t;\delta t)}{\delta t} \end{aligned} \tag{3}$$

where $Q_s(t;\delta t)$ is the volume flux averaged over δt; δV_s is the volume of bed load particle passing through A within δt; $S(t)$ is the cumulative number of particles passing through the cross section since $t = 0$ while $\delta S(t;\delta t)$ is the cumulative number of particles passing through the cross section within δt, i.e., $\delta S(t;\delta t) = S(t+\delta t) - S(t)$ (see Figure 2c); and $v_s = 1/6\pi D^3$ is the volume of a particle and D is the diameter of a particle. Here we drop the parameter v_s (which we take to be constant for any given experiment) for simplicity and define the particle flux of bed load transport as

$$q_s(t;\delta t) = \delta S(t;\delta t)/\delta t \tag{4}$$

This form can be easily transformed into the mass or volume flux of bed load transport by multiplying by the particle mass or volume. Here $q_s(t, \delta t)$ is a random variable. A strict definition of fluctuation of bed load transport flux is thus $q_s' = q_s - \langle q_s \rangle$. Here we simply use $\langle q_s'^2 \rangle$, i.e., the variance of $q_s(t, \delta t)$, to represent the strength of fluctuations.

Based on equation (4), the bed load transport flux can be calculated as the sum of emigration events δS during a given time period δt (see Figure 2c). Emigration is one of the discrete transition events of $N(t)$. Thus, it would be possible to count the number of the transition events, which is also a random variable. In fact, this counting statistics problem has been widely tackled in many scientific fields [*Gopich and Szabo*, 2006; *Ohkubo*, 2008; *Ohkubo*, 2009; *Pilgram et al.*, 2003; *Sinitsyn and Nemenman*, 2007]. Two groups of approaches, i.e., the path integral formulation [*Ohkubo*, 2008, 2009; *Pilgram et al.*, 2003; *Sinitsyn and Nemenman*, 2007] and transition matrix approach [*Gopich and Szabo*, 2006], have been developed. We pursue our theoretical treatment in terms of the path integral formulation, which is closer to the physical origin of stochasticity. It should be noted, however, that the analytical solution for the fluctuations derived from the path integral formulation coincides with the one obtained from the transition matrix approach.

2.1. Stochastic Formulation of the Bed Load Transport Flux

The bed load transport flux is defined by equation (4). Since the statistics of $N(t)$ are known, we can derive the theoretical formulation of the PDF of the bed load transport flux by connecting it to the statistics of $N(t)$. We first discretize time and, correspondingly, the number of moving particles and emigration events in a time interval $[t_i, t_i + \Delta t_i)$ as $\Delta N_i = N(t_i + \Delta t_i) - N(t_i)$, $\Delta S_i = S(t_i + \Delta t_i) - S(t_i)$, and $t_{i+1} = t_i + \Delta t_i$. When $\max\{\Delta t_i\} \to 0$, we have the following governing equations:

$$P[\Delta S_i = 1 | N(t_i) = N_i] = \gamma N_i \mathrm{d}t + o(\mathrm{d}t) \tag{5a}$$

$$P[\Delta S_i = 0 | N(t_i) = N_i] = 1 - \gamma N_i \mathrm{d}t + o(\mathrm{d}t) \tag{5b}$$

As shown in *Ancey et al*. [2008], there exists a time interval that is long enough to allow several emigration events to occur, but sufficiently short so that the number of particles that commence movement and then migrate out of the window within the same interval can be taken to be zero. In this time interval, the PDF of the number of emigration events can be expressed as a binomial distribution with parameter $p_m = 1 - \exp(-\gamma \Delta t)$, i.e.,

$$P[\Delta S_i = k | N(t_i) = N_i] = \frac{N_i!}{k!(N_i - k)!} p_m^k (1 - p_m)^{N_i - k} \tag{6}$$

Pilgram et al. [2003] and *Sinitsyn and Nemenman* [2007] further pointed out that when $N \gg 1$, there exists a timescale Δt (far larger than dt), over which many transitions into and out of N occur, but the fractional change of N is still small, i.e., $1 \ll \Delta N \ll N$. For this condition, the change of the total emigration rates, Δf_3, are also small and all emigration events are uncorrelated and Poissonian as expressed by the relation below

$$P[\Delta S_i = n | N(t_i) = N_i] = \exp[-f_3(N_i)\Delta t] \frac{[f_3(N_i)\Delta t]^n}{n!} \tag{7}$$

As shown in Appendix A, equations (5a), (5b), and (6) can be transformed into equation (7). Thus, equation (7) can be used as a basis for developing a formulation representing the emigration process. Note that the number of emigration events ΔS_i depends only on the status of $N(t_i)$; thus, when the exact state of $N(t_i)$ is known, every value of ΔS_i is conditionally independent of each other.

Equation (7), which pertains to the emigration process at short timescales, is insufficient to connect statistics of S with N analytically. An additional observation can help us obtain this connection readily. We observe that since $\langle N \rangle = \lambda/(\sigma + \gamma - \mu) \sim O(L)$, the total entrainment rate $f_1 = \lambda + \mu N \sim O(L)$ and the total deposition rate $f_2 = \sigma N \sim O(L)$, but $f_3 = \gamma N \sim O(1)$. This indicates that when L is sufficiently large, $f_{i=1,2} \gg f_{i=3}$ and the number of moving particles (N) are dominated by the transition events of $f_{i=1,2}$ and show only weak dependence on $f_{i=3}$, i.e., emigration events S. In other words, N is so large that the emigration events perturb it only minimally, so that $N(t)$ has only a weak dependence on δS. We thus have

$$P\left(\sum \Delta S_i = n | N_1, N_2 \cdots\right) = \exp\left[-\sum f_3(N_i)\Delta t\right] \frac{\left[\sum f_3(N_i)\Delta t\right]^n}{n!} \tag{8}$$

which can be rewritten in continuous form with a path integral as

$$P[\delta S = n | N(t) : t_0 < t < t_0 + \delta t] = \exp\left\{-\int f_3[N(\tau)]\mathrm{d}\tau\right\} \frac{\left[\int f_3[N(\tau)]\mathrm{d}\tau\right]^n}{n!} \tag{9}$$

where $\delta S = S(t_0 + \delta t) - S(t_0)$ and $\delta t = \sum \Delta t_i$. A detailed proof of equation (8) can be found in Appendix B.

Therefore, the probability for $\delta S = n$ is expressed by a conditional expectation as

$$P(\delta S = n) = E\{P[\delta S(t_0, \delta t) = n | N(t) : t_0 < t < t_0 + \delta t]\} = \int \frac{e^{-\alpha}\alpha^n}{n!} P(\alpha, t)\mathrm{d}\alpha \tag{10a}$$

$$\alpha = \int_{t_0}^{t_0 + \delta t} f_3[N(\tau)]\mathrm{d}\tau \tag{10b}$$

where $P(\alpha, t)$ is the PDF of α and $f_3(N(t)) = \gamma N(t)$. Equations (10a) and (10b) define a Cox process (or doubly stochastic Poisson process), where the parameter of a generalized Poisson process α is also a random variable

[*Cox*, 1955]. It represents a superposition of a series of Poisson distributions, taking every possible integral path of $N(t)$ into account. Equations (10a) and (10b) can be tested accurately by the Gillespie algorithm [*Gillespie*, 1991].

Equations (10a) and (10b) together with equation (4) provide a stochastic description of the bed load transport flux, based on counting statistics of emigration events. The structure of the theoretical formulation turns out to be a doubly stochastic process, and more specifically a Poisson process parameterized with the time integral of $N(t)$ [*Cox*, 1955; *Gillespie*, 1991; *Snyder and Miller*, 1991]. To further interpret the Cox process, we start from the simplest case. If the parameter of a Poisson process is constant in time, it represents the simplest homogenous Poisson process, such as the one of the Einstein model. When the governing parameter of a Poisson process is a function of time, the process becomes an inhomogeneous Poisson process. In both cases, the parameters are deterministic functions (or constant). Eventually, when the parameter of a Poisson process is also a random variable, the process becomes a doubly stochastic Poisson process or Cox process. Due to the time integral of $N(t)$, the future state of the system thus depends not only on the present state but also on its history (non-Markovian). These memory mechanisms may be crucial for resolving the features of the scaling relation between fluctuations of bed load transport flux and sampling timescales. Because of the time integral, the analytical solution of equations (10a) and (10b) is difficult to obtain. Nevertheless, the variance of δS, i.e., a measure of the strength of fluctuations, can be analytically derived. We do this in the next subsection.

2.2. Multiregime Fluctuations Over Timescales: Analytical Solution

Equations (10a) and (10b) connect the process δS with the temporal integral of a known process N. Though such a connection does not directly allow an explicit solution of PDF of δS, statistical moments of δS can be straightforwardly derived from equations (10a) and (10b) and moments of α. Equation (11) presents the relation between moments of δS and α:

$$\begin{aligned}\langle n(n-1)\cdots(n-p+1)\rangle_{\delta S} &= \sum_{n=1}^{\infty} n(n-1)\cdots(n-p+1)P(\delta S = n)\\ &= \sum_{n=1}^{\infty}\frac{e^{-\alpha}\alpha^{n-p}}{(n-p)!}\int \alpha^p f(\alpha,t)\mathrm{d}\alpha = \langle \alpha^p\rangle\end{aligned} \tag{11}$$

Thus, we have $\langle n\rangle_{\delta S} = \langle\alpha\rangle$ and $\langle n^2\rangle_{\delta S} - \langle n\rangle_{\delta S} = \langle\alpha^2\rangle$. Correspondingly, $\mathrm{var}(\delta S) = \langle n^2\rangle_{\delta s} - \langle n\rangle_{\delta s}^2 = \mathrm{var}(\alpha) + \langle\alpha\rangle$. Appendix C presents the details of an iterative procedure which can be used to derive analytical expressions of the moment of α up to any order. The analytical expression of var (δS) takes the form as (Appendix C)

$$\begin{aligned}\mathrm{var}[\delta S(\delta t)] &= \langle\alpha(\delta t),\alpha(\delta t)\rangle + \langle\alpha(\delta t)\rangle\\ &= \gamma^2\frac{\lambda(\sigma+\gamma)}{(\sigma+\gamma-\mu)^2}2t_c\left[\delta t - t_c\left(1-e^{-\delta t/t_c}\right)\right] + \frac{\gamma\lambda}{\sigma+\gamma\text{-}\mu}\delta t\end{aligned} \tag{12}$$

where $t_c = 1/(\sigma+\gamma-\mu)$ is the autocorrelation time of $N(t)$, representing the memory timescale of the system, and the autocorrelation function is

$$\rho(\tau) = \frac{\langle N(t_0+\tau), N(t_0)\rangle}{\mathrm{var}(N)} = \exp(-\tau/t_c) \tag{13}$$

where the longer t_c is, the longer is the time over which correlation is sustained [*Ancey et al*., 2008]. The variance of bed load transport flux can be computed from equation (4), i.e., $\mathrm{var}(q_s(\delta t)) = \mathrm{var}(\delta S(\delta t))/\delta t^2$, with unit ($\mathrm{T}^{-2}$).

We transform the parameter $\mathrm{var}(q_s(\delta t))$, which is a decreasing function of δt, into a nondecreasing one by multiplying the two, i.e.,

$$\delta t\cdot\mathrm{var}[q_s(\delta t)] = \gamma^2\frac{\lambda(\sigma+\gamma)}{(\sigma+\gamma-\mu)^2}2t_c\left[1-\frac{t_c}{\delta t}\left(1-e^{-\delta t/t_c}\right)\right] + \frac{\gamma\lambda}{\sigma+\gamma-\mu} \tag{14}$$

Based on the above equation, we can now divide the timescale dependence of variance of bed load transport flux (equation (14)) into three stages, namely, intermittent ($0 < \delta t \ll t_I$), invariant ($t_I < \delta t < t_c$), and memoryless ($\delta t \gg t_c$) stages. These are, respectively, defined as follows:

$$\delta t \cdot \mathrm{var}[q_s(\delta t)] \approx \begin{cases} \dfrac{\gamma\lambda}{\sigma+\gamma-\mu} & 0 < \delta t \ll t_I \\ \delta t \cdot \dfrac{\gamma^2\lambda(\sigma+\gamma)}{(\sigma+\gamma-\mu)^2} & t_I < \delta t < t_c \\ 2\gamma^2 \dfrac{\lambda(\sigma+\gamma)}{(\sigma+\gamma-\mu)^2} t_c + \dfrac{\gamma\lambda}{\sigma+\gamma-\mu} & t_c \ll \delta t < \infty \end{cases} \tag{15}$$

where $t_I = (\sigma+\gamma-\mu)/[\gamma(\sigma+\gamma)]$ denotes the transition timescale from the intermittent stage to the invariant stage, here called the intermittent timescale. Thus, when $\delta t \ll t_I$, bed load transport flux is intermittent: That is, most of the time it has zero value, and rest of the time it has the value of $1/\delta t$, which corresponds to high intermittency since δt is very small. When $\delta t \gg t_c$, the correlation between of the number of moving particles vanishes and the fluctuations become independent. When δt falls into the range $t_I < \delta t < t_c$, $\mathrm{var}(q_s(\delta t)) \cong \gamma^2\lambda(\sigma+\gamma)/(\sigma+\gamma-\mu)^2 = \mathrm{var}(\gamma N(t))$, corresponding to a constant value.

Equation (15) demonstrates that within the intermittent stage, the variance decays with timescale as a power law with exponent -1. Within the memoryless stage, although a power law decay exponent of -1 is also seen, the fluctuation strength is much larger than the one predicted by the recast Einstein model. In addition, due to the vanishing of correlation between the number of moving particles, the fluctuations turn out to be white noise (i.e., a series of independent discrete signals with zero mean and finite variance), where the Central Limit Theorem applies.

Between these two stages, there is, interestingly, a fluctuation-invariant stage, and the strength of fluctuation within it equals the variance of its transition rate function $f_3(N) = \gamma N(t)$, i.e.,

$$\mathrm{var}[q_s(\delta t)] = \mathrm{var}[\gamma N(t)] = \gamma^2\lambda(\sigma+\gamma)/(\sigma+\gamma-\mu)^2$$

Physically, this means that if one simply uses the number of moving particles to evaluate the statistics of bed load transport flux, i.e., $q_s = N(t)\bar{u}_s / L \cong \gamma N(t)$ (where $\bar{u}_s$ is the mean velocity of a particle), the value would be correct only within the fluctuation-invariant stage. For instance, in the intermittent stage, the evaluated variance is underestimated compared with the real variance, and the opposite behavior is shown within the memoryless stage.

2.3. Dimensionless Number for Three-Regime Relation

To gain more insight into the three-regime relation, we further propose a dimensionless number that quantifies the relative strength of fluctuations, as well as the significance of multiregime phenomena. This dimensionless number, *Ra*, is defined as follows:

$$Ra(\delta t) = \frac{\delta t \cdot \mathrm{var}[q_s(\delta t)]}{\mathrm{mean}[q_s(\delta t)]} = \frac{2t_c}{t_I}\left[1 - \frac{t_c}{\delta t}\left(1 - e^{-\delta t/t_c}\right)\right] + 1 \approx \begin{cases} 1 & 0 < \delta t \ll t_I \\ \dfrac{\delta t}{t_I} & t_I < \delta t < t_c \\ \dfrac{2t_c}{t_I} + 1 & t_c \ll \delta t < \infty \end{cases} \tag{16a}$$

$$Ra_m = \max_{\delta t > 0}[Ra(\delta t)] = \frac{2t_c}{t_I} + 1 \tag{16b}$$

Ra describes the three-regime relation between fluctuations of bed load transport processes and sampling timescales under different physical conditions within a common framework. First, *Ra* emphasizes the importance of the sampling timescales, so that it would be meaningless without specifying the sampling timescale when discussing the fluctuation of bed load transport. Second, *Ra* always takes the value of unity at the intermittent stage. This is essential in order to allow direct comparisons of fluctuation strengths under different physical conditions. Third, *Ra* explicitly precludes the influence of mean flux as well as the width effect quantified by λ.

The structure of *Ra* allows the occurrence of an interesting circumstance when comparing fluctuation strengths of two bed load transport processes with each other. Suppose there are two processes having the same mean

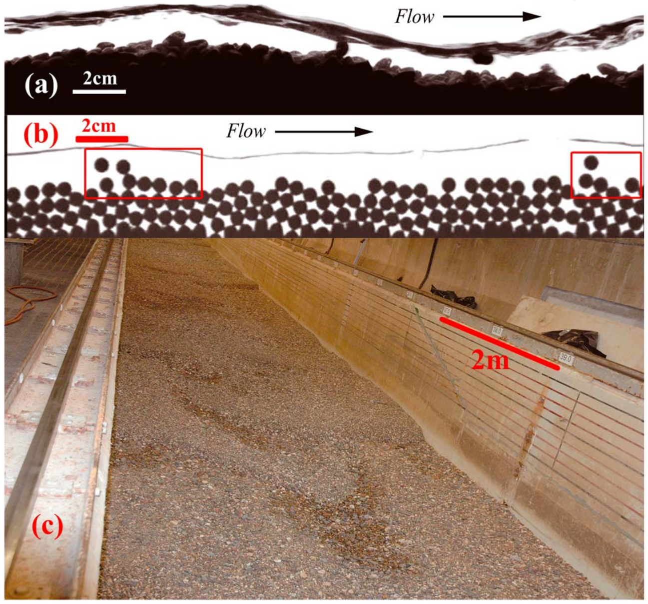

Figure 3. Photographs of bed forms in three experiments. (a) Two-dimensional antidune-covered bed and free surface of P1: elevation varies only along the streamwise direction. (b) Particle clusters of A2. (c) Three-dimensional dunes of S3: bed elevation varies along both the streamwise and spanwise directions.

value of bed load transport flux. Process A has $t_l = 1$ s and $t_c = 10$ s, while Process B has $t_l = 10$ s and $t_c = 200$ s. It is easy to find that at the timescale $\delta t = 10$ s the fluctuation of Process A is larger than Process B, whereas at the timescale $\delta t = 200$ s the fluctuation of Process B is larger than Process A. This means that there is no strength consistency across sampling timescales when comparing the fluctuation strengths of two cases with each other. Thus, a sole comparison of fluctuation strength at one sampling timescale cannot be extendable to other sampling timescales without *Ra*. This further emphasizes the importance of obtaining *Ra* over a broad range of sampling timescales when investigating fluctuations of bed load transport process.

Ra_m is the maximum *Ra* at large sampling timescales (i.e., $\delta t \gg t_c$). Ra_m quantifies both the significance of the three-regime relation and the relative magnitude of fluctuations of bed load transport flux. The larger Ra_m is, the more strongly the statistics of bed load flux shows multiregime behavior, and the stronger the fluctuations are. On the contrary, when $Ra_m = 1$, fluctuation strength versus sampling timescale obeys a single-scaling law relation in which case all the three regimes collapse into one, and the fluctuations are Poissonian.

In the next section, we use three sets of experiments to demonstrate the three-regime behavior predicted by equation (16) and to evaluate the ability of the model to capture this behavior.

3. Experiments

3.1. Experimental Setup and Data Collected

Three experiments are used to investigate the detailed statistics of bed load transport flux [*Ancey et al*., 2006; *Heyman et al*., 2013; *Singh et al*., 2010]. All three experiments concern steady flows with constant particle feed rate. The mean bed load transport flux is under weak and moderate conditions, so that the particles are near the incipient condition for motion and move through frequent saltation rather than intense sheet sliding. In this section, we introduce all three experimental setups, experimentally demonstrate the observation of multiregime fluctuations, and compare them with the theoretical predictions.

The first experiment was conducted in a small-scale channel at Laboratory of Environmental Hydraulics, École polytechnique fédérale de Lausanne, to investigate the bed load transport of monosize particles in supercritical flow (hereafter referred to as P1). The details of the experimental facility can be found in *Heyman et al*. [2013, 2014]. Here we briefly describe the experimental conditions. The flume is 2.5 m long and 8 cm wide. The bed consisted of natural particles which were monosize with a diameter of 8.5 mm. Both output solid discharge and bed elevation were monitored during experiments. The temporal resolution of output solid discharge was about 10^{-1} s, and the data were collected for about 10^5 s. This high temporal resolution allows us to perform statistical analysis over a wide range of scales. The bed exhibited a two-dimensional form, with upstream-migrating antidunes (Figure 3a), and the pattern of upstream migration of the antidunes is illustrated in Figure 4. (Supporting information can be found in *Heyman et al*. [2013].) The mean height H_b, length L_b, and crest celerity C_b of antidunes were 1.0 cm, 25 cm, and 0.2 mm/s, respectively.

In the second experiment (hereafter referred to as A2), *Ancey et al*. [2006] used another steep flume. The bed consisted of monosize spherical particles with a diameter of 6 mm. The channel width was only slightly

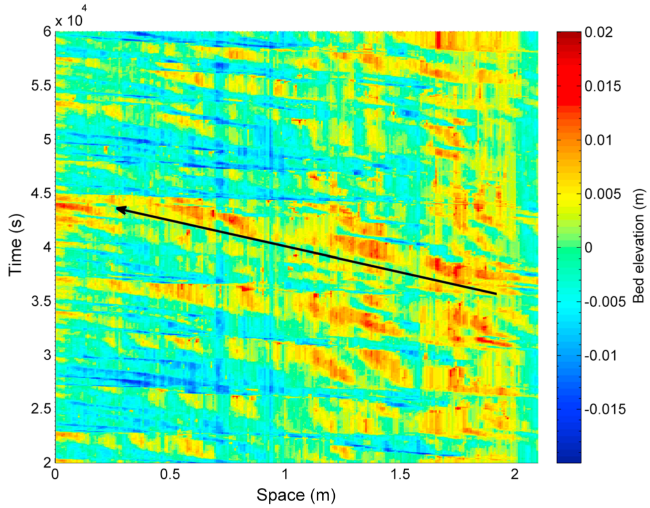

Figure 4. Bed elevation evolution over the entire flume length of P1. The bed elevation variation corresponds to antidunes. Above the black arrow line, an antidune is seen to start from the downstream end of flume and propagate upstream. The figure allows the determination of antidune height and celerity.

greater than the particle diameter. The flow and the bed formation were completely 2-D, preventing any complex 3-D bed forms [*Frey and Church*, 2009]. All the trajectories of moving spherical particles were captured in a fixed window using a high-speed camera. The data have high temporal resolution (about 10^{-2} s) but are limited in time (about 60 s). An examination of the 60 s videos of the experiments reveals collective entrainment and the formation and destruction of intermittent particle clusters (Figure 3b). Collective entrainment serves as a feedback loop for more entrainment, and particle clusters result in correlated patterns of bed load transport, both of which contribute to the long-term correlated motion of bed load particle.

As opposed to the two experiments above, the water flow of the experiments of *Singh et al*. [2010] (hereafter referred to as S3) was subcritical. The experiment was carried out in a large flume with a gentle slope; the flume was 55 m long, 2.74 m wide, and had a maximum depth of 1.8 m, as shown in Figure 2c. The water discharge is 2800 L/s. The average bed load transport flux is much larger in this case than the other two cases. The bed consisted of particles with two separate groups of diameters, with a median diameter of 7.7 mm. The bed load particle accumulation series were 20 h long, with a temporal resolution of 1.1 s. In *Ganti et al*. [2009], it was suggested that 2 min averaging may be needed to remove mechanical noise (due to vibrations of particle weighing pans). The bed was covered with three-dimensional dunes (see Figure 3c). As first demonstrated by *Hino* [1968] for the case of dunes, bed forms show correlated behavior, which implies correlated behavior of the bed load particles that construct them. The mean height H_b, length L_b, and crest celerity C_b of bed forms were 8.34 cm, 3.29 m, and 6.94 mm/s, respectively [*Singh et al*., 2010, 2011, 2012b]. The data allow determination of bed load transport over a multisize bed and may show inherent multiple dynamics of different sized particles because of size-selective particle entrainment and particle inertia. The experiment thus allows testing as to whether the same kind of multiregime relation in bed load transport, as seen in experiments P1 and A2, also holds for Froude-subcritical flow over a bed covered with dunes. All the relevant dimensionless numbers and experimental conditions are shown in Table 1, where τ_b is Shields stress on the bed which is obtained by removing the sidewall stress from the total Shields stress $\tau_t = \bar{h}\sin\theta/D_m/(\rho_s/\rho - 1)$ [*Vanoni*, 1975; *Wong and Parker*, 2006]; $Fr = \bar{u}/\sqrt{g\bar{h}}$ is the Froude number; θ is the slope angle (%); $\bar{u}$ is the mean fluid velocity (m/s); $\bar{h}$ is the mean water depth (cm); and $\bar{q}_s$ is the mean bed load transport flux (particles/s).

Table 1. Experimental Conditions and Dimensionless Number[a]

	τ_b	Fr	θ	$\bar{u}$	$\bar{h}$	$\bar{q}_s$
P1	0.076	1.44	7	0.53	1.37	1.11
A2	0.080	1.37	10	0.41	1.08	6.85
S3	0.132	0.64	0.29	1.59	64	1553.02[b]

[a]Shields stress (τ_b) on the bed which is obtained by removing the sidewall stress from the total Shields stress $\tau_t = \bar{h}\sin\theta/D_m/(\rho_s/\rho - 1)$, as specified by *Vanoni* [1975] and *Wong and Parker* [2006]; $Fr = \bar{u}/\sqrt{g\bar{h}}$ is the Froude number; θ is the slope angle (%); $\bar{u}$ is the mean fluid velocity (m/s); $\bar{h}$ is the mean water depth (cm); and $\bar{q}_s$ is the mean bed load transport flux (particles/s).
[b]Bed load transport flux is calculated from the mass flux and the median diameter of particles.

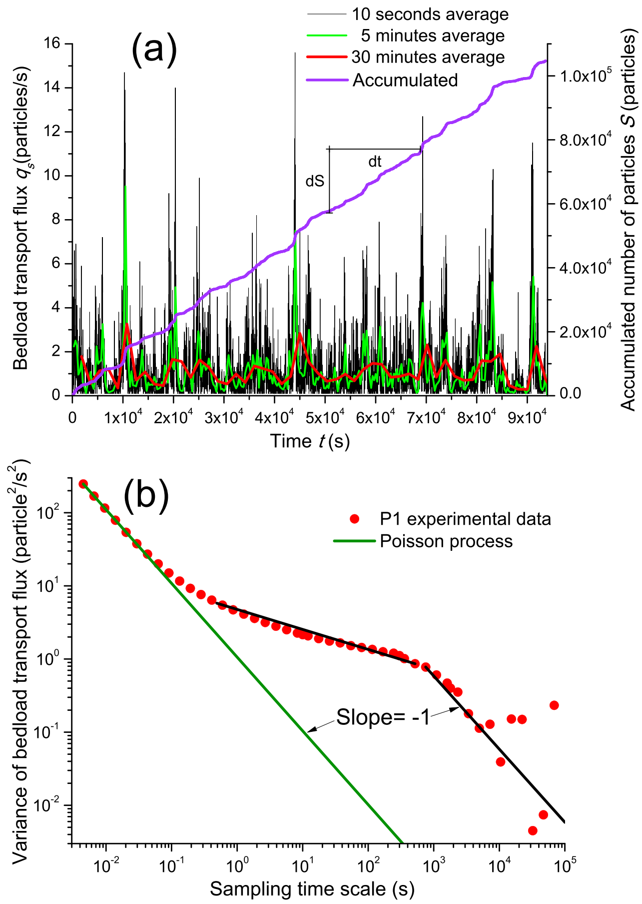

Figure 5. The bed load transport flux series and fluctuations of P1. (a) Stationary series of the bed load transport flux averaged over 10 s (black line), 5 min (green line), 30 min (red line), and the accumulated number of particles (purple line). These series show that the strength of fluctuations decay as sampling scale increases. (b) Variance of bed load transport flux versus sampling time. Einstein's theory, i.e., Poisson process, underestimates the fluctuations and predicts a power law decay relation. Experimental data, however, exhibit the three-stage curve obtained herein.

3.2. Results

3.2.1. Overview of Experimental Multiregime Relation

We first introduce the procedure to obtain the relevant quantities used in the subsequent analysis. The bed load transport flux is calculated by counting how many particles pass through a cross section of the channel in a specified timescale (sampling timescale) as defined by equation (4). Though this definition is commonly used in experiments and field surveys [*Ancey*, 2010; *Gomez and Church*, 1989], the problem of temporal fluctuations arises and restricts its application [*Ancey*, 2010; *Bunte and Abt*, 2005; *Singh et al.*, 2009]. The study herein is motivated precisely by this issue.

In all three experiments used here, high-resolution series of accumulated bed load particles $S(t)$, passing through a measuring cross section, were acquired. Here we divide the duration of the record into equal time intervals, i.e., the sampling timescale δt, and count the incremental number of accumulated bed load particles during each interval δt, i.e., $\delta S(t{,}\delta t) = S(t + \delta t) - S(t)$ (Figure 2c). The series of bed load transport flux q_s can be obtained from equation (4) as shown in Figure 5a. The fluctuation strength sampled in three different timescales (i.e., 10 s, 5 min, and 30 min) clearly decrease as timescale increases (Figure 5a). Let T_m and S be the total duration of measurement and the total number of accumulated particles, respectively. One can verify that the arithmetic mean of $q_s(t, \delta t)$ equals S/T_m, a value which does not change with δt since the whole series is partitioned into equal pieces without overlaps. (We note that this nonoverlapping partitioning was not used in the averaging methods of *Singh et al.* [2009].) We further analyze the experimental data to identify the relations between the variances of bed load transport flux and their sampling timescales. For the sake of clarity, we show the variance of bed load transport flux extracted from the data of P1 in Figure 5b. We present the data from the other two experiments below, in a comparison with the theoretical formulation.

As shown in Figure 5b, the fluctuation strength tends to decrease as the sampling timescale increases, as expected. The slope of the variance of q_s versus δt in double logarithmic coordinate changes with sampling time, so there is no unique scaling law. When the timescale is either sufficiently small or large, there are two separate power law relations between the variance of the bed load transport flux and the sampling timescale, both with scaling exponent -1. A transition stage with a much gentler slope links the two stages. Near the center of the transition stage, the strength of fluctuations decreases only mildly as the timescale increases.

The prediction of the Poisson process model remains accurate only at small sampling timescales. When the sampling timescale increases up to a certain bounding timescale (t_l), the experimental variance starts to deviate from the Einstein model. Another power law stage with a much gentler slope and more fluctuations

Table 2. Measured and Calculated Parameters[a]

	t_c	t_I	Ra_m	λ	σ	μ	γ
P1	181.82	0.49	749.68	2.6767	5.0032	5.00	0.0023
A2	10.00	1.14	18.54	38.09	4.86	4.778	0.0180
S3	125.00	0.0027	92593.59	20.13	4.39	5.00	0.62

[a]The memory timescale is t_c (s); t_I is the intermittent timescale (s); Ra_m is the dimensionless number quantifying the relative strength of fluctuations of bed load transport flux; λ is the individual entrainment rate (s^{-1}); σ is the deposition rate (s^{-1}); μ is the collective entrainment rate (s^{-1}); and γ is the emigration rate (s^{-1}). In P1 and S3, t_c and Ra_m were experimentally measured and μ was set to 5.00 s^{-1}, and then t_I, λ, σ, and γ can be calculated; in A2, nevertheless, t_I and σ were measured and t_c was set to 10 s, and Ra_m, λ, μ, and γ can be calculated.

than the Einstein model emerges and is seen over several orders of magnitude of sampling timescale. In this regime the larger the sampling timescale is, the more is the variance. When the sampling timescale increases beyond a second turning point (t_c), a third power law stage with scaling exponent -1 shows, within which the variances are orders of magnitude larger than the ones predicted by Einstein model. At the largest timescales (e.g., $\delta t > 3$ h), there are too few data to estimate a reliable variance. This is a likely reason for the scatter in this region apparent in Figure 5b.

Qualitatively, the experimental multiregime relation coincides with the theoretical prediction very well. To gain a quantitative description, the model parameters need to be estimated first.

3.2.2. Estimation of Parameters

Equations (16a) and (16b) can be used to predict multiregime relations, once the four parameters (i.e., λ, μ, σ, and γ) are obtained. In the *Ancey et al.* [2008] model, the deposition rate σ was directly measured and the other three parameters were inferred from the measurement of the statistics of $N(t)$. Equations (16a) and (16b), on the other hand, provide three relations for the four unknown parameters, based on the pattern of Ra. Therefore, if one parameter is determined independently, the other three can be computed from the theory.

Of the four parameters λ, μ, σ, and γ, the easiest one to measure directly is σ. Thus, the straightforward way to test the theory would be to use an experimentally determined value of σ, evaluate λ, μ, and γ from the theory, and then test the theory against the data. In the cases of experiments P1 and S3, however, the measurements needed to determine σ were not taken. In addition, in the case of experiment A2, although σ was measured, the lack of information necessary to estimate t_c results in one more tunable parameter. With this in mind, we choose μ in P1 and S3 and t_c in A2 as a tunable parameter to test the theory. The measured and calculated parameters are listed in Table 2. It is straightforward to design future experiments which would provide enough information to make this tuning unnecessary.

Note that the current estimation method is an alternative for which only the data of the cross sectionally averaged flux are available to use. A rigorous calibration based on imaging techniques may provide a better basis for the development and testing of stochastic formulations. In addition, predictive relations between the parameters λ, σ, λ, and μ and parameters governing the hydraulics of the flow need to be developed.

3.2.3. Comparison Between Theory and Experiments

As shown in Figure 6, the theoretical formula, in general, agrees well with the experimental data in all three cases. As predicted by the theory, three stages of the multiregime relation can be identified, in particular in the case of P1. The A2 data were acquired from a high-speed camera which had a high temporal resolution (10^{-2} s); but the duration of the record was not long enough to completely represent the invariant stage or any of the memoryless stage behavior; thus, the memory timescale t_c can be neither obtained experimentally nor calculated solely from other parameters related to the experimental results for bed load transport flux, such as $\langle q_s \rangle$ and t_I. When the timescale is large (e.g., $\delta t > 10$ s), the variable data are not reliable, since the measurement duration is not long enough to accurately compute them. If unreliable points in the range $\delta t > 10$ s are excluded, the agreement with theory is good and, in addition, the degree of agreement between the theory and experiment is independent of t_c as it ranges from 5 s to infinity, so the memory time for A2 is simply set to 10 s. The S3 data, on the other hand, is sufficiently long to approach the memoryless stage, but the temporal resolution (about 1.1 s) is so low that only part of the invariant stage could be identified. In addition, the intermittent stage could not be resolved. Because the memory timescale t_c could be obtained from the data for this experiment, however, it was possible to compute t_I from the relation $t_I = 2t_c/(Ra_\mathrm{m} - 1)$.

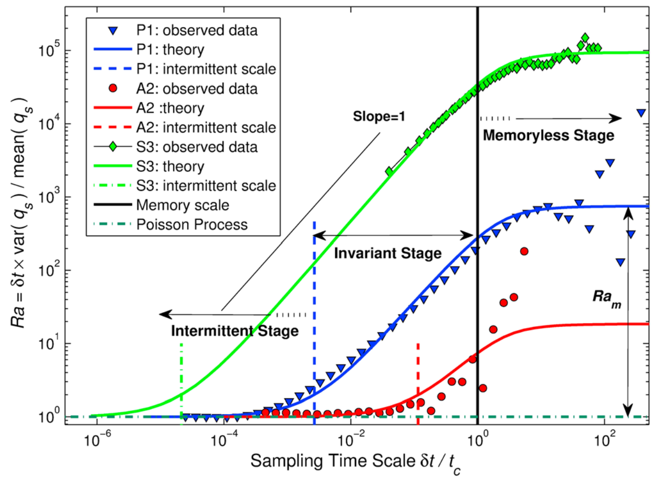

Figure 6. Dimensionless variance $Ra = \delta t \cdot \mathrm{var}[q_s(\delta t)]/\mathrm{mean}[q_s(\delta t)]$ of bed load transport flux $q_s(\delta t)$ versus dimensionless sampling timescale. Ra is divided into three stages demarcated by an intermittent timescale (t_I) and a memory timescale (t_c). The three stages are the intermittent stage($\delta t \ll t_I$), the invariant stage($t_I < \delta t < t_c$), and the memoryless stage ($\delta t \gg t_c$), respectively. $Ra_{\mathrm{m}} = \max\{Ra\} = 2t_c/t_I + 1$. For P1, $t_c = 181.82$ s and $t_I = 0.49$ s. For A2: $t_c = 10$ s and $t_I = 1.14$ s. For S3: $t_c = 125$ s and $t_I = 0.0027$ s. The three stages and the value of Ra_{m} for P1 are labeled in the figure. The value of t_c for A2 cannot be inferred from the experiment or calculated by the theory, and thus is taken as 10 s. The precise value of t_c has no influence on the agreement between experiment and theory as long as $t_c > 5$ s.

It is important to point out that herein only one new element, i.e., collective entrainment, which lumps correlated behavior of particle motion due to a wide range of physical mechanisms, has been added to the classical Einsteinian model. It is this single addition that gives rise to the rich pattern of multiregime behavior documented here.

4. Discussion

4.1. The Physical Origin of t_c and t_I

As shown above, the dimensionless number Ra and Ra_{m} can well describe the three-regime relation. Ra and Ra_{m} consist of two essential characteristic timescales, t_c and t_I. The physical origin and significance of parameters t_c and t_I are worth discussing.

The value of t_c is obtained from the autocorrelation function (equation (13)) of the number of moving particles. This mathematically reveals the crucial influence of correlated motion of bed load transport on multiregime behavior. In the *Ancey et al.* [2008] theory, the main source of correlation comes from collective entrainment, i.e., moving particles colliding and destabilizing static particles and producing more moving particles. Collective entrainment acts as a feedback loop; and thus, μ is a key parameter controlling the internal correlation of the system [*Ancey et al.*, 2008; *Ancey*, 2010]. In addition to collective entrainment, however, there remain numerous mechanisms that can also result in correlated motion of bed load particles. To understand these mechanisms more fully, an analysis of the dynamics of particle motion is needed.

Since bed load transport is a typical two-phase flow system, particles are driven by the forces of the fluid field, such as the drag force, lift force, and related continuous forces [*Fu et al.*, 2005; *Zhong et al.*, 2011], as well as forces associated with particle motion and interaction, such as collective entrainment produced by random collisions among moving particles and destabilization of bed forms under shear flow. Such behavior may induce long-term correlated motion of particles [*Ancey et al.*, 2008; *Gomez et al.*, 1989; *Heyman et al.*, 2013; *Staron et al.*, 2006]. Turbulent flow, including uncorrelated random fluctuations [*Fu et al.*, 2005; *Zhong et al.*, 2011] and large coherent eddy structures [*Drake et al.*, 1988], acts to destabilize particles and entrain them into motion. In multisized sediment, bed load entrainment and emigration rates vary according to particle size, and are also correlated to each other by factors such as hiding [*Ganti et al.*, 2010; *Hassan and Church*, 2000]. At low bed load transport rates, the intermittent formation and disintegration of microform clusters creates correlated fluctuations [*Strom et al.*, 2004]. Finally, when the bed organizes itself into bed forms, the migration of these bed forms creates correlated motions [*Gomez et al.*, 1989; *Hamamori*, 1962; *Hino*, 1968; *Nordin*, 1971; *Singh et al.*, 2011]. In the text below, we use the term “cluster” in a generic sense, to describe any parcel of particles with correlated motion, from collective entrainment and microclusters to dunes and antidunes.

Correlated transport acts differently. Correlated patterns of particle motion indicate that the history of motion (e.g., particle collisions, particle cluster formation and disintegration, local destabilization in zones of locally higher slope, eddy bursts, and interaction between grains of different sizes and bed form migration) can influence particles such that their motion is no longer independent; the motion at any given time may be stimulated (or suppressed) by the history of movement of a bed load particle. In principle, t_c should be associated with the longest correlated timescale among these mechanisms. In addition, the geometry of the boundary may also influence the autocorrelation of bed load transport. Although *Ra* is explicitly independent of mean flux and the width effect parameterized by λ, the influence of physical geometry or boundary on the fluctuations might be implicitly included in the parameter μ. For instance, when the channel width is very large, μ may be constant as well as Ra_m, even though the width varies. On the contrary, when the channel width is relatively small, the width effect may influence the formation of bed forms [*Crickmore*, 1970] and thus may influence the values of μ, t_c, and *Ra*. Similarly, although the several mechanisms described above that are not explicitly included in the *Ancey et al*. [2008] theory can also cause correlated motion of bed load particles, we assume that correlation induced by all these clustering mechanisms can be simply lumped into μ in our study.

When $\mu = 0$, $Ra_m = 2\gamma/(\sigma + \gamma) + 1 \cong 1$, yielding the power law relation predicted by the recast Einstein model. On the other hand, when $\mu \to \sigma + \gamma$, t_c and Ra_m are very large (t_c, $Ra_m \to \infty$) and the long memory time leads to a wide range of the invariant stage (t_I, t_c). Thus, a plot of the range of three stages, i.e., (0, t_I), (t_I, t_c), and (t_c, ∞), is most clearly expressed in terms of logarithmic coordinates. These predictions of the theoretical formulation further emphasize the importance of the correlated motion of particles on the three-regime relation.

Meanwhile, the discrete nature of bed load particle motion needs to be emphasized in order to understand the physics of the intermittent stage and its characteristic timescale t_I. It can be expected that when the sampling timescale is sufficiently small, particles intermittently cross the counting plane, and such motion can induce an instantaneous flux up to $1/\delta t$, which appears as a series of spikes bounded by long zones of vanishing flux. It is for this reason that we call this stage the intermittent stage. The flux becomes a discrete process, and the sampled time series can be seen as a series of Bernoulli trials (only 0 or 1 particle crosses the plane during δt). The Bernoulli distribution with a very low occurrence probability has a variance equal to its mean, so that the variance of the bed load transport flux also converges to the ratio of mean flux to δt at sufficiently small timescales. Thus, at this scale different modes of particle motion cannot be distinguished. The timescale dependence of the variance of bed load transport flux at the intermittent stage is expressed as a power law with scaling exponent -1. The intermittent stage consisting of a series of Bernoulli trials is simple. If assuming that the Bernoulli trials are independent, we obtain a white noise process in every sampling timescale, which leads to an overall power law with scaling exponent -1. But the existence of correlations between Bernoulli trials results in the nonlinear superposition of microscopically simple behaviors, which can create more complex, fascinating phenomena at the macroscopic scale. The parameter t_I quantifies the boundary between the intermittent stage and invariant stage. As the timescale increases up to t_I, there can be more than one particle passing through the cross section in a given time interval, allowing more fluctuations. Thus, t_I denotes the smallest time gap between emigration particles in the case of cluster transport of moving particles. For instance, if the coherent eddy structure is responsible for a cluster pattern of transport of moving particles [*Drake et al*., 1988], t_I could be a ratio of a minimum timescale of coherent eddy structure to the number of massive moving particles carried by the eddy. Therefore, assuming the turbulent energy of the coherent eddy structure to be invariant, the finer a particle is, the more often it would be put in motion, so that a smaller value of t_I would be expected. These local features, such as compactness or composition of granular bed, may have more influence on t_I than global features.

In summary, t_c and t_I represent the correlated motion and discrete nature of bed load particles, respectively. Among all the correlated motion mechanisms, t_c should be associated with the longest correlated timescale, whereas t_I denotes the smallest time gap between emigration particles in the case of cluster transport of moving particles. The two characteristic timescales govern the three-regime relation. At the intermittent stage, the sampled flux is a discrete process (either 0 or $1/\delta t$) and its variance is suppressed. Different modes of particle motion can no longer be distinguished. The timescale dependence of the variance of bed load transport flux at the intermittent stage takes the form of a power law with scaling exponent -1. At the invariant stage, due to the correlated motions of bed load particles, the flux may sometimes rise abruptly or remain static for some time [*Nikora et al*., 2002]. This results in large fluctuations around the mean. When the correlated motion of particles is dominant, the larger the timescale, the higher is the probability that an abrupt peak occurs. Therefore, although a larger sampling timescale can smooth the fluctuations of the bed load transport flux, it allows more abrupt peaks and concomitantly more fluctuations. The two effects compete to balance each other, so that the strength of fluctuations in this stage is insensitive to sampling time. Lastly, each type of correlated particle motion has its own characteristic memory time (i.e., autocorrelation time), such that when the timescale is much larger than a characteristic memory timescale t_c, the possibility of abrupt peaks becomes vanishingly small. Beyond this scale, fluctuations become not only memoryless but also single scaling with exponent -1.

4.2. Implications of Experiments

Taking a closer look at Figure 6, we can distinguish the three experiments in terms of different curves of Ra versus $\delta t/t_c$ and different values of Ra_m. Interestingly, experiment S3, which has a subcritical flow condition and the largest bed load transport flux, has the largest value of Ra_m. Insofar, as the conditions of this experiment most closely resemble low-slope sand-bed rivers, this result suggests that such rivers may have larger fluctuations of bed load transport flux than in mountain gravel-bed rivers, which P1 and A2 more closely resemble. This result suggests a trend that is opposite to previous studies [*Ancey et al*., 2006; *Barry*, 2004; *Bohm et al*., 2004; *Martin*, 2003; *Wilcock*, 2001].

To investigate the reason, we recall the expression $Ra_m = 2t_c/t_I + 1$. S3 has a much shorter intermittent timescale t_I than P1 and A2, indicating a much closer time gap between two migrating particles within a cluster of particles in transport. In the case of S3, the bed material consists of grains with two separate populations of diameters, with the finer grains more easily entrained into transport [*Hassan and Church*, 2000]. Thus, t_I may be much shorter than other experimental cases, so giving rise to a very large value of $Ra_m = 2t_c/t_I + 1$. In other words, the tremendously large Ra_m of S3 results from the variability of grain size. If we were to conduct an experiment with a bimodal mixture of grain sizes, but with other conditions the same as A2 (or P1), the intermittent time might turn out to be smaller than A2 (or P1) and Ra_m might be larger than S3.

One can also verify that among all possible correlated scales, the characteristic timescale of bed form migration $t_b = L_b/C_b$ is the closest to the experimental memory time of P1 and S3. For these experiments, other correlated timescales are smaller than t_b by several orders of magnitude. For instance, in P1, t_b is 1250 s and t_c is 181.82 s; in S3, t_b is 474.0 s and t_c is 125 s. In addition, in S3 the average time between two consecutive bed form crests is 883.8 s [*Singh et al*., 2012a], i.e., a value that is larger than t_b. Both values of t_b for P1 and S3 (as well as the average time gap between two crests of consecutive bed forms in S3) are larger, but not beyond an order of magnitude above t_c, so satisfying the condition $\delta t \gg t_c$ for the memoryless stage. In regard to A2, it remains difficult to quantify the timescale for the life cycle of clusters (formation to disintegration) for the purposes of comparison. Having said this, however, the above observations indicate that (1) the memory scale derived from the stochastic theory is indeed consistent with the corresponding physical phenomena; and (2) in P1 and S3, the dominant correlated timescales correspond to the characteristic timescale of bed form migration.

5. Conclusion

In this study, we explore how the sampling timescale influences the fluctuations of bed load transport flux. We adopt the *Ancey et al*. [2008] theory of stochastic dynamics of bed load transport to develop a theoretical formulation for the PDF of bed load transport flux. We obtain an analytical solution for the variance of the bed load transport flux versus sampling time. The solution agrees well with available experimental data in the literature. Of particular interest is the fact that the solution exhibits a three-regime behavior of fluctuations of bed load transport flux, rather than the single regime of the classical Einstein formulation.

We show that the three-regime relation consists of three piecewise power law relations demarcated by an intermittent timescale and a memory timescale. The intermittent timescale corresponds to the time gap between two adjacent particles in cluster transport (which may range from clusters of a few particles up to dunes and antidunes), and the memory timescale is the longest correlation time of particle transport. The multiregime model reduces to a (recast) form of the Einstein model in the limit as the parameter $\mu = 0$, corresponding to a power law relation with an exponent of -1. The Einstein formulation, however, accurately predicts the variance of bed load transport flux only at timescales less than the intermittent timescale. When the timescale increases beyond the intermittent timescale, the variance of bed load transport flux becomes invariant with respect to the timescale and can be well represented by the statistics of the number of moving particles. The range of the invariant stage depends on the ratio of the memory timescale to the intermittent timescale. In the limit as the sampling timescale increases well beyond the memory timescale, another power law with an exponent of -1 appears.

The three-regime relation may result from both the discrete nature of bed load particles and their correlated motion. While our model describes the three-regime relation as a result of temporal correlation of the number of moving particles, it does not account for the details of the physical mechanisms that drive correlations at different scales. Many possible mechanisms may be responsible, including collective entrainment, particle cluster formation and disintegration, interaction between the motion of grains of different size, coherent turbulent structure, local avalanche behavior, and bed form migration. We present preliminary results showing that correlated particle motion due to bed form migration contributes to the longest memory scale and captures most of the fluctuations in experiments P1 and S3. A formulation that fully accounts for the underlying physics is a worthwhile future goal.

It is also worth inquiring as to the connection between the temporal statistics and the corresponding spatial statistics of bed load transport. It would be of value to try to connect the present three-regime scaling relation to the three spatial ranges of particle anomalous diffusion first described by *Nikora et al*. [2002] and elaborated upon by *Martin et al*. [2012]. The recent work achieved by *Ancey and Heyman* [2014] and *Heyman et al*. [2014] has shed light on the characteristics of bed load dynamics from a spatial point of view. They found that the fluctuation of the spatial average of the number of moving particles over different length scales takes the same form as the variation of *Ra* over different timescales [*Heyman et al*., 2014]. An examination of the *Heyman et al*. [2014] experimental data, however, shows that Taylor's frozen-flow hypothesis fails to transform the spatial variance of the bed load transport flux into the temporal one. It remains an open question as to how one should connect the temporal and spatial statistics of bed load transport flux effectively.

In terms of practical applications, the three-regime relation presented here provides the basis for a tool for designing appropriate measuring strategies for bed load transport flux. An appropriate temporal resolution up to the memory scale might be both necessary and sufficient to capture the detailed statistics of bed load transport. The pursuit of high-resolution data of bed load transport flux is no longer an endless task but a sufficiently long measuring duration, i.e., long enough to obtain a reliable determination of the variance of bed load transport flux as the sampling timescale becomes as large as $10t_c$ is still required to fully describe the memoryless stage.

Appendix A: Poisson Distribution for the Number of Emigration Events in Short Time Interval

In previous studies we can find two types of PDF besides the Poisson distribution to express the number of emigration events in short time intervals. In this appendix, we show that in short time intervals both types of PDF (equations (5a), (5b), and (6)) can be transformed into a Poisson distribution (equation (7)).

Equations (5a) and (5b) are the governing equations to connect the statistics of the number of moving particle $N(t)$ with the total number of emigration events in infinitesimal time dt, i.e., ΔS.

$$P[\Delta S_i = 1|N(t_i) = N_i] = \gamma N_i \mathrm{d}t + o(\mathrm{d}t) \tag{5a}$$

$$P[\Delta S_i = 0|N(t_i) = N_i] = 1 - \gamma \mathrm{d}t + o(\mathrm{d}t) \tag{5b}$$

When $\Delta t = \mathrm{d}t \to 0$, we have

$$\exp(-\gamma N_i \Delta t) = 1 - \gamma N_i \mathrm{d}t + o(\mathrm{d}t) \tag{A1}$$

Substituting equation (A1) into equation (7), we can obtain

$$P[\Delta S_i = 1|N(t_i) = N_i] = \gamma N_i \mathrm{d}t + o(\mathrm{d}t) \tag{A2a}$$

$$P[\Delta S_i = 0|N(t_i) = N_i] = 1 - \gamma N_i \mathrm{d}t + o(\mathrm{d}t) \tag{A2b}$$

$$P[\Delta S_i \geq 2|N(t_i) = N_i] = o(\mathrm{d}t) \tag{A2c}$$

which are the same as equations (5a) and (5b). This demonstrates the equality between equations (5a), (5b), and (7).

As proved in *Ancey et al*. [2008], there exists a time interval that is long enough to allow several emigration events to occur but sufficiently short so that the number of particles that start moving and then migrate out of the window within the same interval can be approximated as zero. In this time interval, the PDF of the number of emigration events can be expressed as a binomial distribution with parameter $p_m = 1 - \exp(-\gamma\Delta t)$, i.e.,

$$P[\Delta S_i = k | N(t_i) = N_i] = \frac{N_i!}{k!(N_i - k)!} p_m^k (1 - p_m)^{N_i - k} \tag{6}$$

To deal with the factorial of a large number, we use Stirling's approximation:

$$N_i! \sim \sqrt{2\pi N_i}\left(\frac{N_i}{e}\right)^{N_i}, \qquad (N_i - k)! \sim \sqrt{2\pi(N_i - k)}\left(\frac{N_i - k}{e}\right)^{N_i - k} \tag{A3}$$

Similar to equation (A1), $p_m = 1 - \exp(-\gamma\Delta t) \sim \gamma\Delta t$. Substituting p_m and equation (A3) into equation (6), we have

$$\begin{aligned} P[\Delta S_i = k | N(t_i) = N_i] &\cong \sqrt{\frac{N_i}{N_i - k}}\left(1 - \frac{k}{N_i - k}\right)^{N_i - k} e^k \exp[-(N_i - k)\gamma\Delta t]\frac{(N_i\gamma\Delta t)^k}{k!} \\ &\cong \exp[-N_i\gamma\Delta t]\frac{(N_i\gamma\Delta t)^k}{k!} \end{aligned} \tag{A4}$$

where the following conditions are used (1) Δt is a short time interval; (2) k cannot be arbitrarily large, because otherwise the trivial result, $P[\Delta S_i = k | N(t_i) = N_i] = 0$ is obtained due to the term $p_m^k \sim O(\Delta t^k) \ll 1$; and (3) N_i is sufficiently large to satisfy the condition $N_i \gg k$. Equation (A4) is precisely the same as equation (7). This demonstrates the equality between equations (6) and (7).

Appendix B: Proof of the Weak Dependence of *N* on *S*

A stochastic process described by a master equation can be simulated exactly by *Gillespie* [1991] algorithm, and the number of emigration events obey the conditional Poissonian with average $f_3(N_i)\Delta t$, provided N_i is unchanged during Δt, as in equation (4). In the Gillespie algorithm, one transition event changes the state of the system (i.e., N_i), and then the next transition event must be evaluated by using the updated state. However, if we let Δt become small enough, it becomes possible that there is at most one transition event in each step, i.e., $\Delta S_i \in \{0, 1\}$. Equation (4) remains correct and the conditional independence of each step in equation (4) can also hold without the assumption of the independence of either ΔS_i or N_i.

Another issue concerning the Gillespie algorithm arises in regard to the derivation of equations (5a) and (5b). The independence of each subequation does not allow equations (5a) and (5b) to hold directly, because the definition of conditional independence is as follows.

$$\Pr(A \cap B | Y) = \Pr(A|Y)\Pr(B|Y) \tag{B1}$$

Thus, to obtain equations (5a) and (5b), we need to verify the proposition that equation (B2) below holds.

B1. Proposition

As L is sufficiently large, the following equation holds

$$P(\Delta S_i = n | N(t_i) = N_i) ? = P(\Delta S_i = n | N_1, N_2, N_3 \cdots) \tag{B2}$$

Before proving the *proposition*, we first list some observations, which are helpful to understand the *proof*.

Since $N(t_i)$ is Markovian and ΔS_i is a subevent of $N(t_i)$, we have

$$P(\Delta S_i = n | N_1, N_2 \cdots) = P(\Delta S_i = n | N_i, N_{i+1}) \tag{B3}$$

Substituting equation (B3) into equation (B2), the proposition can be cast as

$$P(\Delta S_i = n | N_i) ? = P(\Delta S_i = n | N_i, N_{i+1}) \tag{B4}$$

As documented in the body of paper, if we assume N_{i+1} has no dependence on ΔS_i, we can obtain equation (B4) directly. Each of three transition events of $N(t)$, $f_i(N)(i = 1,2,3)$, has the following respective transition rate over Δt: i.e., $(\lambda + \mu N)\Delta t \sim O(L)\Delta t$, $\sigma N\Delta t \sim O(L)\Delta t$, and $\gamma N\Delta t \sim O(1)\Delta t$. We can find that the total emigration rate $f_3(N)$ is much smaller than that of other two events when L is sufficiently large, so that the other two transition events dominate. In other words, N is so large ($\langle N\rangle = \lambda/(\sigma+\gamma-\mu) \sim O(L)$) that the emigration events ($\langle \delta S\rangle = \gamma\lambda/(\sigma+\gamma-\mu) \sim O(1)$) perturb it only minimally. Therefore, $N(t)$ has only a weak dependence on δS. The procedures of this proof are as follows. First, we show both sides of equation (B4) on an equal base in explicit form and then we show that the difference between the two sides vanishes as L grows sufficiently large.

Table B1. Terms of $P(\Delta S_i = n|N_i = n_i)P(N_{i+1} = n_{i+1}|N_i = n_i)$

	$\Delta S_i = 0$	$\Delta S_i = 1$
$N_{i+1} = N_i - 1$	$(\sigma+\gamma)N_i\Delta t + o(\delta t)$	$o(\delta t)$
$N_{i+1} = N_i$	$1 - [\lambda + (\sigma + 2\gamma + \mu)N_i]\Delta t + o(\Delta t)$	$\gamma N_i\Delta t + o(\delta t)$
$N_{i+1} = N_i + 1$	$(\lambda + N_i\mu)\Delta t + o(\delta t)$	$o(\delta t)$

B2. Proof of the Proposition

The left-hand side (LHS) of equation (B4) is transformed as

$$P(\Delta S_i = n|N_i) = \frac{P(N_i = n_i)}{P(N_i = n_i, N_{i+1} = n_{i+1})}P(\Delta S_i = n|N_i = n_i)P(N_{i+1} = n_{i+1}|N_i = n_i) \tag{B5}$$

The RHS of equation (B4) can then be transformed to

$$P(\Delta S_i = n|N_i, N_{i+1}) = \frac{P(N_i = n_i)}{P(N_i = n_i, N_{i+1} = n_{i+1})}P(\Delta S_i = n, N_{i+1} = n_{i+1}|N_i = n_i) \tag{B6}$$

We now let Δt become small enough so that for all i, $|N_i - N_{i+1}| \le 1$. Note that the first factor on the RHS of equation (B5) is the same as the one in equation (B6). Thus, to prove equation (B2), we need only to compare the remaining terms, the RHS of equations (B5) and (B6), with each other to see whether the difference vanishes as L is sufficiently large. Table B1 lists the product of the second and third factors on the RHS of equation (B5), and Table B2 lists the second factor on the RHS of equation (B6). Table B3 lists the differences between Tables B1 and B2.

From Table B3, we can find that the difference is of the same order as or less than $\gamma N_i\Delta t$.

Because $\gamma \sim O(1/L)$, we have

$$|P(\Delta S_i = n|N_i) - P(\Delta S_i = n|N_i, N_{i+1})| \le \frac{P(N_i = n_i)N_i\Delta t}{P(N_i = n_i, N_{i+1} = n_{i+1})}O(1/L) \tag{B7}$$

Thus, the difference between the two sides of equation (B2) becomes vanishingly small as L becomes sufficiently large.

Appendix C: Statistical Moments of the Time Integral of N

Let $\tilde{\alpha}(t) = \tilde{\alpha}(t|t_0) = \int_{t_0}^{t} N(\tau)\mathrm{d}\tau$ be the time integral of the Markov process $N(t)$ [*Gillespie*, 1991], defined as

$$\tilde{\alpha}(t + \mathrm{d}t) = \tilde{\alpha}(t) + N(t)\mathrm{d}t + o(\mathrm{d}t) \tag{C1}$$

whose m order moment can be obtained by calculating m power of equation (C1)

$$\tilde{\alpha}^m(t + \mathrm{d}t) = \tilde{\alpha}^m(t) + m\tilde{\alpha}^{m-1}(t)N(t)\mathrm{d}t + o(\mathrm{d}t) \tag{C2}$$

Averaging this equation yields

$$\langle\tilde{\alpha}^m(t + \mathrm{d}t)\rangle = \langle\tilde{\alpha}^m(t)\rangle + m\langle\tilde{\alpha}^{m-1}(t)N(t)\rangle\mathrm{d}t + o(\mathrm{d}t) \tag{C3}$$

Taking the limit $\mathrm{d}t \to 0$, we thus arrive at the set of moment equations:

$$\frac{\mathrm{d}}{\mathrm{d}t}\langle\tilde{\alpha}^m(t)\rangle = m\langle\tilde{\alpha}^{m-1}(t)N(t)\rangle \tag{C4}$$

The initial conditions are $\langle\alpha^m(t_0)\rangle = 0$. However, the cross moments on the RHS of equation (C4) still need to be

Table B2. Terms of $P(\Delta S_i = n, N_{i+1} = n_{i+1}|N_i = n_i)$

	$\Delta S_i = 0$	$\Delta S_i = 1$
$N_{i+1} = N_i - 1$	$\sigma N_i\Delta t + o(\Delta t)$	$\gamma N_i\Delta t + o(\Delta t)$
$N_{i+1} = N_i$	$1 - [\lambda + (\sigma + \gamma + \mu)N_i]\Delta t + o(\Delta t)$	$o(\Delta t)$
$N_{i+1} = N_i + 1$	$(\lambda + N_i\mu)\Delta t + o(\Delta t)$	$o(\Delta t)$

Table B3. Terms of the Differences: $P(\Delta S_i = n | N_i = n_i)P(N_{i+1} = n_{i+1} | N_i = n_i) - P(\Delta S_i = n, N_{i+1} = n_{i+1} | N_i = n_i)$

	$\Delta S_i = 0$	$\Delta S_i = 1$
$N_{i+1} = N_i - 1$	$\gamma N_i \Delta t + o(\Delta t)$	$-\gamma N_i \Delta t + o(\Delta t)$
$N_{i+1} = N_i$	$-\gamma N_i \Delta t + o(\Delta t)$	$\gamma N_i \Delta t + o(\Delta t)$
$N_{i+1} = N_i + 1$	$o(\Delta t)$	$o(\Delta t)$

closed. To do this, we need the propagating expression of N(t):

$$N(t + \mathrm{d}t) = N(t) + \Xi[\mathrm{d}t; N(t), t] \quad \text{(C5)}$$

where $\Xi(\mathrm{d}t; N(t), t)$ is the stochastic propagator function of $N(t)$. $\Xi(\mathrm{d}t; N(t), t)$ represents the stochastic increment of $N(t)$ in dt. In the present study,

$$P[\Xi(\mathrm{d}t; N(t), t) = 1] = (\lambda + \mu N)\mathrm{d}t + o(\mathrm{d}t) \quad \text{(C6a)}$$

$$P[\Xi(\mathrm{d}t; N(t), t) = 0] = 1 - [\lambda + (\mu + \sigma + \gamma)N]\mathrm{d}t + o(\mathrm{d}t) \quad \text{(C6b)}$$

$$P[\Xi(\mathrm{d}t; N(t), t) = -1] = (\sigma + \gamma)N\mathrm{d}t + o(\mathrm{d}t) \quad \text{(C6c)}$$

Multiplying equations (C2) by (C5), we have

$$\begin{aligned}\widetilde{\alpha}^m(t + \mathrm{d}t)N(t + \mathrm{d}t) &= \widetilde{\alpha}^m(t)N(t) + m\widetilde{\alpha}^{m-1}(t)N^2(t)\mathrm{d}t \\ &\quad + \widetilde{\alpha}^m(t)\Xi(\mathrm{d}t; N(t), t) + o(\mathrm{d}t)\end{aligned} \quad \text{(C7)}$$

Averaging equation (3.12) and taking the limit d$t \to 0$, we have

$$\frac{\mathrm{d}}{\mathrm{d}t}\langle\widetilde{\alpha}^m(t)N(t)\rangle = m\langle\widetilde{\alpha}^{m-1}(t)N^2(t)\rangle + \langle\widetilde{\alpha}^m(t)B_1(N(t), t)\rangle \quad \text{(C8)}$$

where $B_1(N(t), t) = \lambda + (\mu - \sigma - \gamma)N(t)$ is the first order moment of the propagator.

With equations (C4) and (C8), one can deduce any order moment of the time integral of $\gamma N(\tau)$.

Let $m = 1$; substituting into equation (C8), one can obtain

$$\frac{\mathrm{d}}{\mathrm{d}t}\langle\widetilde{\alpha}(t), N(t)\rangle = \mathrm{var}(N(t)) + (u - \sigma - \gamma)\langle\widetilde{\alpha}(t), N(t)\rangle \quad \text{(C9)}$$

where var[$N(t)$] is the steady variance of $N(t)$ [*Ancey et al*., 2008], which can be expressed as

$$\mathrm{var}(N(t)) = \frac{\lambda(\sigma + \gamma)}{(\sigma + \gamma - \mu)^2} \quad \text{(C10)}$$

Then solving equation (C9), we can obtain the cross moment as

$$\langle\widetilde{\alpha}(t), N(t)\rangle = \frac{\lambda(\sigma + \gamma)}{(\sigma + \gamma - \mu)^2}[1 - \exp(-t/t_c)] \quad \text{(C11)}$$

where $t_c = 1/(\sigma + \gamma - \mu)$.

Substituting equation (C11) into equation (C4), the variance of $\widetilde{\alpha}$ can be obtained by equation (C12).

$$\mathrm{var}(\widetilde{\alpha}) = 2\int_{t_0}^{t}\langle\widetilde{\alpha}(t), N(t)\rangle\mathrm{d}s \quad \text{(C12)}$$

The full expression of the variance of $\alpha(t)$ is

$$\mathrm{var}[\alpha(\delta t)] = \gamma^2\,\mathrm{var}(\widetilde{\alpha}) = \gamma^2\frac{\lambda(\sigma + \gamma)}{(\sigma + \gamma - \mu)^2}2t_c\left[\delta t - t_c\left(1 - e^{-\delta t/t_c}\right)\right] \quad \text{(C13)}$$

and thus the variance of $\delta S(\delta t)$ is

$$\begin{aligned}\mathrm{var}[\delta S(\delta t)] &= \mathrm{var}[\alpha(\delta t)] + \langle\alpha(\delta t)\rangle \\ &= \gamma^2\frac{\lambda(\sigma + \gamma)}{(\sigma + \gamma - \mu)^2}2t_c\left[\delta t - t_c\left(1 - e^{-\delta t/t_c}\right)\right] + \frac{\gamma\lambda}{\sigma + \gamma - \mu}\delta t\end{aligned} \quad \text{(C14)}$$

Notation

C_b mean crest celerity of bed form migration, [LT^{-1}].

C_v coefficient of variation.

D	diameter of bed load particle [L].
$f_i(N)$	total transition rates of ith event, [T^{-1}], where $f_1(N)$ is the total entrainment rate, $f_2(N)$ is the total deposition rate, and $f_3(N)$ is the total emigration rate.
H_b	mean length of bed forms, [L].
Fr	$Fr = \bar{u}/\sqrt{g\bar{h}}$ Froude number.
$\bar{h}$	mean water depth, [L].
L, L_b	length of the elementary window; mean length of bed forms, [L].
mean(*)	mean value of *.
$N(t)$	moving particle number in the elementary window.
P(*)	probability distribution function of *.
p_m	probability of one moving particle migrating out of a window in Δt.
Q_s	volume flux of bed load transport, [L^{3}T^{-1}].
q_s, $\bar{q}_s$	particle flux of bed load transport and its mean value, [T^{-1}].
Ra, Ra_m	dimensionless number characterizing multiregime, and its corresponding maximum value.
$S(t)$	accumulative emigration particle number.
t_c, t_I, t_b, T_m	memory timescale, intermittent timescale, characteristic timescale of bedfrom migration, and measurement duration, respectively, [T].
$\bar{u}$, $\bar{u}_s$	mean fluid velocity; mean particle velocity, [LT^{-1}].
var(*)	variance of *.
W	channel width, [L].
α	time integral of $N(t)$ process, [T].
τ_b, τ_t	dimensionless bed/total shear stress; $\tau_t = \bar{h}\sin\theta/D_m/(\rho_s/\rho - 1)$, where τ_b is obtained after sidewall correction of τ_t, see *Vanoni* [1975] and *Wong and Parker* [2006].
θ	channel slope (%).
λ	individual entrainment rate of the whole observation window, [T^{-1}].
μ	collective entrainment rate, [T^{-1}].
σ	deposition rate, [T^{-1}].
γ	emigration rate, [T^{-1}].
$\langle X\rangle$	mean of random variable X.
$\langle A, B\rangle$	covariance of random variable A and B.

Acknowledgments

The work presented here was supported by the Swiss National Science Foundation under grants 200021-129538 ("The Stochastic Torrent: Stochastic model for bed load transport on steep slope") and 200021-105193/1 ("Transient free-surface flows of concentrated suspensions—Application to geophysical flows," funded by an R'Equip grant). The National Natural Science Foundation of China under grant 51379100 also financially supported this work. We thank Professor Efi Foufoula-Georgiou (University of Minnesota) for her constructive preview of our work. We also thank Professors Simon Tait (University of Sheffield) and Vladimir Nikora (University of Aberdeen) for their helpful suggestions. We appreciate the help of Arvind Singh (University of Minnesota), who provided insightful reviews and details concerning his experiments (S3). Raleigh Martin (UCLA) and an anonymous reviewer are also appreciated for their constructive reviews. We thank the editorial team for their thorough and constructive remarks. Experiments, P1 and A2, can be requested from Joris Heyman (joris.heyman@epfl.ch) and Christophe Ancey (christophe.ancey@epfl.ch), respectively.

References

Ancey, C. (2010), Stochastic modeling in sediment dynamics: Exner equation for planar bed incipient bed load transport conditions, *J. Geophys. Res.*, *115*, F00A11, doi:10.1029/2009JF001260.

Ancey, C., and J. Heyman (2014), A microstructural approach to bedload transport: Mean behavior and fluctuations of particle transport rates, *J. Fluid Mech.*, *744*, 129–168, doi:10.1017/jfm.2014.74.

Ancey, C., T. Bohm, M. Jodeau, and P. Frey (2006), Statistical description of sediment transport experiments, *Phys. Rev. E*, *74*(1), 011302, doi:10.1103/Physreve.74.011302.

Ancey, C., A. C. Davison, T. Bohm, M. Jodeau, and P. Frey (2008), Entrainment and motion of coarse particles in a shallow water stream down a steep slope, *J. Fluid Mech.*, *595*, 83–114, doi:10.1017/S0022112007008774.

Ballio, F., V. Nikora, and S. E. Coleman (2014), On the definition of solid discharge in hydro-environment research and applications, *J. Hydraul. Res.*, *52*(2), 173–184, doi:10.1080/00221686.2013.869267.

Barchyn, T. E., R. L. Martin, J. F. Kok, and C. H. Hugenholtz (2014), Fundamental mismatches between measurements and models in aeolian sediment transport prediction: The role of small-scale variability, *Aeolian Res.*, doi:10.1016/j.aeolia.2014.07.002.

Barry, J. J. (2004), A general power equation for predicting bed load transport rates in gravel bed rivers, *Water Resour. Res.*, *40*, W10401, doi:10.1029/2004WR003190.

Bohm, T., C. Ancey, P. Frey, J. L. Reboud, and C. Ducottet (2004), Fluctuations of the solid discharge of gravity-driven particle flows in a turbulent stream, *Phys. Rev. E*, *69*(6), 061307, doi:10.1103/Physreve.69.061307.

Bradley, D. N., G. E. Tucker, and D. A. Benson (2010), Fractional dispersion in a sand bed river, *J. Geophys. Res.*, *115*, F00A09, doi:10.1029/2009JF001268.

Bunte, K., and S. R. Abt (2005), Effect of sampling time on measured gravel bed load transport rates in a coarse-bedded stream, *Water Resour. Res.*, *41*, W11405, doi:10.1029/2004WR003880.

Campagnol, J., A. Radice, and F. Ballio (2012), Scale-based statistical analysis of sediment fluxes, *Acta Geophys.*, *60*(6), 1744–1777, doi:10.2478/s11600-012-0028-6.

Carey, W., and D. Hubbell (1986), Probability distributions for bedload transport, in *Proceedings of the Fourth Federal Interagency Sedimentation Conference*, Las Vegas, Nev.

Cox, D. R. (1955), Some statistical methods connected with series of events, *J. Roy. Stat. Soc. B. Stat. Meth.*, *17*(2), 129–164.

Crickmore, M. J. (1970), Effect of flume width on bed-form characteristics, *J. Hydraul. Div.*, *96*, 473–496.

Drake, T. G., R. L. Shreve, W. E. Dietrich, P. J. Whiting, and L. B. Leopold (1988), Bedload transport of fine gravel observed by motion-picture photography, *J. Fluid Mech.*, *192*, 193–217, doi:10.1017/S0022112088001831.
Einstein, H. A. (1937), Der Geschiebetrieb als Wahrscheinlichkeitsproblem, Mitt. Versuchsanst. Wasserbau Eidg. Tech. Hochsch. Zürich, Rascher, Zürich, Switzerland.
Einstein, H. A. (1950), The bed-load function for sediment transportation in open channel flows, *Tech*, *Rep*. *1026*. U. S. Department of Agriculture, Washington, D. C.
Ergenzinger, P., C. Jong, J. Laronne, and I. Reid (1994), Short term temporal variations in bedload transport rates: Squaw Creek, Montana, USA and Nahal Yatir and Nahal Estemoa, Israel, in *Dynamics and Geomorphology of Mountain Rivers*, edited by P. Ergenzinger and K.-H. Schmidt, pp. 251–264, Springer, Berlin.
Foufoula-Georgiou, E., and C. Stark (2010), Introduction to special section on Stochastic Transport and Emergent Scaling on Earth's surface: Rethinking geomorphic transport—Stochastic theories, broad scales of motion and nonlocality, *J. Geophys. Res.*, *115*, F00A01, doi:10.1029/2010JF001661.
Frey, P., and M. Church (2009), How river beds move, *Science*, *325*(5947), 1509–1510, doi:10.1126/science.1178516.
Frey, P., C. Ducottet, and J. Jay (2003), Fluctuations of bed load solid discharge and grain size distribution on steep slopes with image analysis, *Exp. Fluids*, *35*(6), 589–597, doi:10.1007/s00348-003-0707-9.
Fu, X. D., G. Q. Wang, and X. J. Shao (2005), Vertical dispersion of fine and coarse sediments in turbulent open-channel flows, *J. Hydraul. Eng.-ASCE*, *131*(10), 877–888, doi:10.1061/(asce)0733-9429(2005)131:10(877).
Furbish, D. J., P. K. Haff, J. C. Roseberry, and M. W. Schmeeckle (2012), A probabilistic description of the bed load sediment flux: 1. Theory, *J. Geophys. Res.*, *117*, F03031, doi:10.1029/2012JF002353.
Ganti, V., A. Singh, P. Passalacqua, and E. Foufoula-Georgiou (2009), Subordinated Brownian motion model for sediment transport, *Phys. Rev. E*, *80*(1), 011111, doi:10.1103/PhysRevE.80.011111.
Ganti, V., M. M. Meerschaert, E. Foufoula-Georgiou, E. Viparelli, and G. Parker (2010), Normal and anomalous diffusion of gravel tracer particles in rivers, *J. Geophys. Res.*, *115*, F00A12, doi:10.1029/2008JF001222.
Gillespie, D. T. (1991), *Markov Processes: An Introduction for Physical Scientists*, Academic Press, San Diego, Calif.
Gomez, B., and M. Church (1989), An assessment of bed-load sediment transport formulas for gravel bed rivers, *Water Resour. Res.*, *25*(6), 1161–1186, doi:10.1029/WR025i006p01161.
Gomez, B., R. L. Naff, and D. W. Hubbell (1989), Temporal variations in bedload transport rates associated with the migration of bedforms, *Earth Surf. Processes Landforms*, *14*(2), 135–156, doi:10.1002/esp.3290140205.
Gopich, I. V., and A. Szabo (2006), Theory of the statistics of kinetic transitions with application to single-molecule enzyme catalysis, *J. Chem. Phys.*, *124*, 154712, doi:10.1063/1.2180770.
Hamamori, A. (1962), A theoretical investigation on the fluctuations of bedload transport, *Rep*, *R4*, 14 Delft Hydraul. Lab., Delft, Netherlands.
Hassan, M. A., and M. Church (2000), Experiments on surface structure and partial sediment transport on a gravel bed, *Water Resour. Res.*, *36*(7), 1885–1895, doi:10.1029/2000WR900055.
Heyman, J., F. Mettra, H. B. Ma, and C. Ancey (2013), Statistics of bedload transport over steep slopes: Separation of time scales and collective motion, *Geophys. Res. Lett.*, *40*, 128–133, doi:10.1029/2012GL054280.
Heyman, J., H. B. Ma, F. Mettra, and C. Ancey (2014), Spatial correlations in bed load transport: Evidence, importance, and modelling, *J. Geophys. Res. Earth Surface*, *119*, 1751–1767, doi:10.1002/2013JF003003.
Hino, M. (1968), Equilibrium-range spectra of sand waves formed by flowing water, *J. Fluid Mech.*, *34*(3), 565–573.
Hoey, T. (1992), Temporal variations in bedload transport rates and sediment storage in gravel-bed rivers, *Prog. Phys. Geogr.*, *16*(3), 319–338, doi:10.1177/030913339201600303.
Martin, R. L., D. J. Jerolmack, and R. Schumer (2012), The physical basis for anomalous diffusion in bed load transport, *J. Geophys. Res.*, *117*, F04001, doi:10.1029/2012JF002608.
Martin, R. L., T. E. Barchyn, C. H. Hugenholtz, and D. J. Jerolmack (2013), Timescale dependence of aeolian sand flux observations under atmospheric turbulence, *J. Geophys. Res. Atmos.*, *118*, 9078–9092, doi:10.1016/j.aeolia.2014.07.002.
Martin, Y. (2003), Evaluation of bed load transport formulae using field evidence from the Vedder River, British Columbia, *Geomorphology*, *53*(1-2), 75–95, doi:10.1016/S0169-555x(02)00348-3.
Nikora, V., H. Habersack, T. Huber, and I. McEwan (2002), On bed particle diffusion in gravel bed flows under weak bed load transport, *Water Resour. Res.*, *38*(6), 1081, doi:10.1029/2001WR000513.
Nordin, C. F. (1971), Statistical properties of dune profiles, U.S. Gov. Print. Off., Washington, D. C.
Ohkubo, J. (2008), The stochastic pump current and the non-adiabatic geometrical phase, *J. Stat. Mech: Theory Exp.*, *2008*(02), P02011, doi:10.1088/1742-5468/2008/02/P02011.
Ohkubo, J. (2009), Variational principle of counting statistics in master equations, *Phys. Rev. E*, *80*(1), 012101, doi:10.1103/PhysRevE.80.012101.
Phillips, J. D. (2010), The job of the river, *Earth Surf. Processes Landforms*, *35*(3), 305–313, doi:10.1002/esp.1915.
Phillips, J. D. (2011), Emergence and pseudo-equilibrium in geomorphology, *Geomorphology*, *132*(3-4), 319–326, doi:10.1016/j.geomorph.2011.05.017.
Pilgram, S., A. N. Jordan, E. V. Sukhorukov, and M. Buttiker (2003), Stochastic path integral formulation of full counting statistics, *Phys. Rev. Lett.*, *90*(20), 206801, doi:10.1103/Physrevlett.90.206801.
Recking, A., F. Liebault, C. Peteuil, and T. Jolimet (2012), Testing bedload transport equations with consideration of time scales, *Earth Surf. Processes Landforms*, *37*(7), 774–789, doi:10.1002/esp.3213.
Sherman, D. J., and B. Li (2012), Predicting aeolian sand transport rates: A reevaluation of models, *Aeolian Res.*, *3*(4), 371–378, doi:10.1016/j.aeolia.2011.06.002.
Singh, A., K. Fienberg, D. J. Jerolmack, J. Marr, and E. Foufoula-Georgiou (2009), Experimental evidence for statistical scaling and intermittency in sediment transport rates, *J. Geophys. Res.*, *114*, F01025, doi:10.1029/2007JF000963.
Singh, A., F. Porte-Agel, and E. Foufoula-Georgiou (2010), On the influence of gravel bed dynamics on velocity power spectra, *Water Resour. Res.*, *46*, W04509, doi:10.1029/2009WR008190.
Singh, A., S. Lanzoni, P. R. Wilcock, and E. Foufoula-Georgiou (2011), Multiscale statistical characterization of migrating bed forms in gravel and sand bed rivers, *Water Resour. Res.*, *47*, W12526, doi:10.1029/2010WR010122.
Singh, A., E. Foufoula-Georgiou, F. Porté-Agel, and P. R. Wilcock (2012a), Coupled dynamics of the co-evolution of gravel bed topography, flow turbulence and sediment transport in an experimental channel, *J. Geophys. Res.*, *117*, F04016, doi:10.1029/2011JF002323.
Singh, A., M. Guala, S. Lanzoni, and E. Foufoula-Georgiou (2012b), Bedform effect on the reorganization of surface and subsurface grain size distribution in gravel bedded channels, *Acta Geophys.*, *60*(6), 1607–1638, doi:10.2478/s11600-012-0075-z.
Sinitsyn, N. A., and I. Nemenman (2007), Universal geometric theory of mesoscopic stochastic pumps and reversible ratchets, *Phys. Rev. Lett.*, *99*(22), 220408, doi:10.1103/PhysRevLett.99.220408.

Snyder, D. D. L., and M. I. Miller (1991), *Random Point Processes in Time and Space*, Springer, New York.

Staron, L., F. Radjai, and J. P. Vilotte (2006), Granular micro-structure and avalanche precursors, *J. Stat. Mech. Theory E*, P07014, doi:10.1088/1742-5468/2006/07/P07014.

Strom, K., A. Papanicolaou, N. Evangelopoulos, and M. Odeh (2004), Microforms in gravel bed rivers: Formation, disintegration, and effects on bedload transport, *J. Hydraul. Eng. ASCE*, *130*(6), 554–567, doi:10.1061/(ASCE)0733-9429(2004)130:6(554).

Stumpf, M. P., and M. A. Porter (2012), Critical truths about power laws, *Science*, *335*(6069), 665–666, doi:10.1126/science.1216142.

Turowski, J. M. (2011), Probability distributions for bed form-dominated bed load transport: The Hamamori distribution revisited, *J. Geophys. Res.*, *116*, F02017, doi:10.1029/2010JF001803.

Vanoni, V. A. (Ed.) (1975), Sedimentation Engineering, *ASCE Manuals and Reports on Engineering Practice 54*, ASCE, New York.

Wilcock, P. R. (2001), Toward a practical method for estimating sediment-transport rates in gravel-bed rivers, *Earth Surf. Processes Landforms*, *26*(13), 1395–1408, doi:10.1002/Esp.301.

Wong, M., and G. Parker (2006), Reanalysis and correction of bed-load relation of Meyer-Peter and Müller using their own database, *J. Hydraul. Eng. ASCE*, *132*(11), 1159–1168, doi:10.1061/(ASCE)0733-9429(2006)132:11(1159).

Zhong, D. Y., G. Q. Wang, and Y. Ding (2011), Bed sediment entrainment function based on kinetic theory, *J. Hydraul. Eng. ASCE*, *137*(2), 222–233, doi:10.1061/(Asce)Hy.1943-7900.0000299.

